Radial dependence of the angular momentum density of a paraxial optical vortex

V. V. Kotlyar, A. A. Kovalev, and A. P. Porfirev
Image Processing Systems Institute of RAS—Branch of the FSRC "Crystallography and Photonics" RAS, Samara, 443001, Russia and Samara National Research University, Samara, 443086, Russia

(Received 21 March 2018; published 23 May 2018)

We obtain general analytic expressions for the linear and angular momentum density of an elliptically polarized paraxial laser beam. As a partial case, we obtain expressions for the linear and angular momentum density of a paraxial elliptically polarized optical vortex. It is shown that for an arbitrary vortex field with rotational symmetry and with circular polarization the effect of the "angular tractor" takes place, which means that the flux of light energy rotates around the optical axis clockwise or counterclockwise at different radii in the beam cross section. It is also shown that the axial component of the angular momentum density of the vortex light field changes its sign at the same radii in the beam cross section. Microparticles trapped in the vortex Bessel beam at different radii are experimentally shown to rotate simultaneously clockwise and counterclockwise.

DOI: 10.1103/PhysRevA.97.053833

I. INTRODUCTION

The orbital angular momentum (OAM) of a light field was introduced into optics 25 years ago [1], but the vortex laser beams carrying OAM have not lost their relevance until now. In the first paper about the OAM of a paraxial light field, a formula was obtained for the OAM density of the Laguerre-Gaussian beams [2]. However, there is no general formula for the OAM density of an arbitrary circularly polarized paraxial field in Ref. [2]. There is only a general formula for the linear momentum density of an arbitrary paraxial light field. It was shown in Ref. [3] that for the Laguerre-Gaussian beam (LG) the azimuthal projection of the linear momentum density vector is proportional to the product of the optical vortex topological charge n and the spin factor $\sigma = \pm 1$, which determines left or right circular polarization of light. Thus, a spin-orbital interaction of the LG beams in free space was demonstrated. In Ref. [4], total linear and angular momenta (AM) were studied for arbitrary nonparaxial laser beams. In Ref. [5], exact equations are given for the distribution of the Poynting vector (PV) and of the AM density of a symmetrical nonparaxial Bessel beam with circular polarization. In Ref. [6], the AM of a sharply converging Gaussian beam was considered. It has been shown numerically that when a circularly polarized Gaussian beam is sharply focused, its spin AM partially transforms into the orbital AM. This is because the electric field in the focus has the increased longitudinal component, which carries a unit topological charge $E_z(r,\varphi) = E_0(r,z)\exp(i\sigma\varphi)$. In Ref. [7], the AM of a vortex Gaussian beam in the sharp focus area is also theoretically considered. It is shown that for $n \geqslant 2$ and $\sigma = -1$, an inverse flux of light energy takes place near the optical axis with respect to the direction of the light beam. The inverse energy flux with respect to the beam propagation direction is called the "optical tractor" [8]. In Ref. [9], a formula was obtained for the total OAM of a Gaussian beam with an embedded optical vortex shifted from the optic axis. Approximate formulas for the PV and AM of nonparaxial LG beams were obtained in Ref. [10]. In Ref. [11], exact expressions are obtained for the AM of vectorial Hankel beams with circular polarization. In Ref. [12], expressions for the AM of a vectorial linearly polarized Gaussian optical vortex are obtained in the form of a series. In Ref. [13], the behavior of PV and AM for the beams of the "swallowtail" type is numerically studied. In Ref. [14], the OAM of paraxial Hankel-Bessel beams [15] is investigated. Note that another approach and another definition of AM and OAM are used in Ref. [16]. In Ref. [16] instead of the Poynting vector $\mathbf{S} = c\,\mathrm{Re}[\mathbf{E}^* \times \mathbf{H}]$, where c is the speed of light, and $\mathbf{E}$ and $\mathbf{H}$ are the electric and magnetic field strength vectors, the canonical momentum density $\mathbf{P} = 0.5\mathrm{Im}[\mathbf{E}^*\nabla\mathbf{E} + \mathbf{H}^*\nabla\mathbf{H}]$ is introduced. Therefore, all the expressions related with the AM look different from the usual consideration [2,3].

From this brief review of the papers related with the OAM theory, it is clear that a general formula for the AM density of an arbitrary paraxial laser beam with circular polarization was not obtained. In this paper, we obtain general expressions for the linear and AM densities of an arbitrary paraxial laser beam with elliptical polarization. Using these expressions, we analyze in detail the effect of the "angular tractor," when the transverse energy flux (or the azimuthal projection of the linear momentum vector) at different distances from the optical axis rotates either clockwise or counterclockwise for the fixed values of the topological charge n and spin parameter σ. This phenomenon was briefly studied in Ref. [7] for circularly polarized Gaussian beams. Here we (i) study it for arbitrary beams, including non-Gaussian ones, and (ii) show that this effect is impossible for linearly polarized beams. It is also shown that the axial projection of the AM density vector changes its sign according to the change in the rotation direction of the transverse energy flux.

II. LINEAR MOMENTUM OF A PARAXIAL LASER BEAM

Now we obtain an expression for the linear momentum of a paraxial light field with elliptical polarization. Let the transverse Cartesian components E_x and E_y of the electric field strength vector $\mathbf{E}$ be related as follows:

$$E_y = i\sigma E_x, \tag{1}$$

 ©2018 American Physical Society

where σ is an arbitrary complex number, for example, $\sigma = 1$ for right circular polarization and $\sigma = -1$ for left circular polarization. The longitudinal component E_z of the electric vector can be found from the Maxwell's equation of continuity $\mathrm{div}\mathbf{E} = 0$:

$$E_z = \frac{i}{k}\frac{\partial E_x}{\partial x} - \frac{\sigma}{k}\frac{\partial E_x}{\partial y}, \tag{2}$$

with the condition that $\partial E_z/\partial z \approx ikE_z$, where k is the wavenumber of light. The time-averaged linear momentum density of the light field reads as

$$\mathbf{p} = \tfrac{1}{2}\mathrm{Re}[\mathbf{E}^* \times \mathbf{H}]. \tag{3}$$

Projections of the magnetic field strength vector $\mathbf{H}$ can be obtained from the Maxwell's equation for a monochromatic field with a cyclic frequency ω (magnetic permeability $\mu = 1$):

$$\nabla \times \mathbf{E} = i\omega\mathbf{H}. \tag{4}$$

Thus, projections of the magnetic vector read as

$$\begin{aligned} H_x &\approx \frac{-i}{\omega}\left(\frac{\partial E_z}{\partial y} + k\sigma E_x\right) \approx -\frac{ik\sigma}{\omega}E_x, \\ H_y &\approx \frac{-i}{\omega}\left(ikE_x - \frac{\partial E_z}{\partial x}\right) \approx \frac{k}{\omega}E_x, \\ H_z &= \frac{-i}{\omega}\left(i\sigma\frac{\partial E_x}{\partial x} - \frac{\partial E_x}{\partial y}\right). \end{aligned} \tag{5}$$

Substituting Eqs. (1), (2), and (5) into Eq. (3), we obtain an expression for the linear momentum density of an elliptically polarized paraxial light field:

$$\begin{aligned} \mathbf{p} = {} & \frac{-i}{4\omega}(1+|\sigma|^2)(E_x^*\nabla E_x - E_x\nabla E_x^*) \\ & -\frac{\mathrm{Re}\sigma}{2\omega}(E_x^*\nabla_\perp E_x + E_x\nabla_\perp E_x^*) \\ & +\frac{k}{2\omega}(1+|\sigma|^2)|E_x|^2\mathbf{z}, \end{aligned} \tag{6}$$

where

$$\nabla = \mathbf{x}\frac{\partial}{\partial x} + \mathbf{y}\frac{\partial}{\partial y}, \quad \nabla_\perp = -\mathbf{x}\frac{\partial}{\partial y} + \mathbf{y}\frac{\partial}{\partial x}.$$

In Eq. (6), $\mathbf{x}$, $\mathbf{y}$, and $\mathbf{z}$ are unit vectors along the Cartesian coordinate axes. At $\sigma = 0$ (linear polarization), Eq. (6) coincides with the known expression from [2,3]. The difference between Eq. (6) and the similar expression for the linear momentum in Ref. [2] is in the second term. Instead of the term $E_x^*\nabla_\perp E_x + E_x\nabla_\perp E_x^*$ in Eq. (6), in Ref. [2] there is the term $[\partial|A(r,z)|^2/\partial r]\boldsymbol{\varphi}$. However, it can be shown that

$$E_x^*\nabla_\perp E_x + E_x\nabla_\perp E_x^* = -\frac{1}{r}\frac{\partial|E_x|^2}{\partial\boldsymbol{\varphi}}\mathbf{r} + \frac{\partial|E_x|^2}{\partial r}\boldsymbol{\varphi},$$

where $\mathbf{r}$, $\boldsymbol{\varphi}$ are the unit vectors along the polar coordinates.

Thus, an expression from [2] was obtained for the linear momentum density of a paraxial beam with a rotationally symmetrical intensity distribution $|E_x| = A(r,z)$.

Expression (6) is a general expression for the linear momentum (or for the Umov-Poynting vector $\mathbf{S}$, since $\mathbf{S} = c\mathbf{p}$, where c is the speed of light in vacuum) and it can be specified for an optical vortex with the following complex amplitude:

$$E_x = A(r,z)\exp(in\varphi), \tag{7}$$

where (r, φ, z) are the cylindrical coordinates. In the cylindrical coordinates, the nabla operators from Eq. (6) read as

$$\nabla = \mathbf{r}\frac{\partial}{\partial r} + \boldsymbol{\varphi}\frac{\partial}{r\partial\varphi}, \quad \nabla_\perp = -\mathbf{r}\frac{\partial}{r\partial\varphi} + \boldsymbol{\varphi}\frac{\partial}{\partial r}, \tag{8}$$

Then, for the linear momentum of an elliptically polarized paraxial optical vortex instead of Eq. (6), we get

$$\begin{aligned} \mathbf{p} = {} & \frac{1+|\sigma|^2}{4c}F\mathbf{r} \\ & +\frac{1}{2\omega}\left[\frac{n}{r}(1+|\sigma|^2)|A(r,z)|^2 - \mathrm{Re}\sigma\frac{\partial|A(r,z)|^2}{\partial r}\right]\boldsymbol{\varphi} \\ & +\frac{1+|\sigma|^2}{2c}|A(r,z)|^2\mathbf{z}, \end{aligned} \tag{9}$$

where

$$F = \frac{-i}{k}\left(A^*\frac{\partial A}{\partial r} - A\frac{\partial A^*}{\partial r}\right).$$

From Eq. (9) follows that the flux of light energy (or a linear momentum) for the paraxial light fields is always directed along the beam propagation:

$$p_z = \frac{1+|\sigma|^2}{2c}|A(r,z)|^2, \tag{10}$$

and there is no effect of the reverse propagation of the energy flux (the effect of the tractor [8]). But from Eq. (9) it follows that the optical vortices have an "angular tractor." This phenomenon was briefly noted in Ref. [7]. Below, this property is considered in more detail.

It is interesting that for the beams, whose phase of the radial part $A(r, z)$ in Eq. (7) does not depend on r, and therefore $F = 0$, there is no energy flow [and a linear momentum (9)] along the radial component. That is, such beams are modes and propagate without diffraction. The Bessel beam is an example of such a diffraction-free vortex laser beam: $A(r,z) = J_n(k_r r)\exp(ik_z z)$, where $J_n(k_r r)$ is the Bessel function; k_r, k_z are the transverse and longitudinal components of the wave vector. An opposite example, used in Ref. [14], is the divergent paraxial Hankel-Bessel vortex beam [15]. For such beams, the energy flux along the radial coordinate is nonzero, and the function F is also different from zero, because the phase of their amplitude function (7) depends on r:

$$A(r,z) = H_{n/2}^{(1)}\left(kz + \frac{kr^2}{4z}\right)J_{n/2}\left(\frac{kr^2}{4z}\right), \tag{11}$$

where $H_{n/2}^{(1)}(x)$ is the Hankel function of the first kind of the semi-integer order.

Now we explain what is meant above by the words "angular tractor." It is seen in Eq. (9) that in the cross section of the vortex beam the energy moves along a circle, since the linear momentum vector has a nonzero azimuthal projection:

$$p_\varphi = \frac{1}{2\omega}\left[\frac{n}{r}(1+|\sigma|)^2|A(r,z)|^2 - \mathrm{Re}\sigma\frac{\partial|A(r,z)|^2}{\partial r}\right]. \tag{12}$$

Moreover, as seen in Eq. (12), if polarization is not linear ($\sigma \neq 0$), then the azimuthal projection of the linear momentum vector can change its sign; that is, the energy flux at different radii in the beam cross section rotates clockwise or counterclockwise for the fixed values of n and σ. In the case of circular polarization ($\sigma = \pm 1$), the equation for the radii, where the azimuthal linear momentum projection changes its sign, has the form

$$\frac{2n}{\sigma}|A(r,z)|^2 = r\frac{\partial|A(r,z)|^2}{\partial r}. \tag{13}$$

III. ANGULAR MOMENTUM OF A PARAXIAL LASER BEAM

Knowing the linear momentum (6) of a paraxial light field, it is possible to obtain an explicit analytic expression for the angular momentum,

$$\mathbf{j} = \mathbf{r} \times \mathbf{p}, \tag{14}$$

of an arbitrary paraxial light field $\mathbf{E}$ with elliptical polarization:

$$\begin{aligned}\mathbf{j} = {} & \frac{-i}{4\omega}(1+|\sigma|^2)z(E_x^*\nabla_\perp E_x - E_x\nabla_\perp E_x^*) \\ & + \frac{\mathrm{Re}\sigma}{2\omega}z(E_x^*\nabla E_x + E_x\nabla E_x^*) + \frac{1+|\sigma|^2}{2c}|E_x|^2\mathbf{e} \\ & + \left[\frac{i}{4\omega}(1+|\sigma|^2)(E_x^*\nabla E_x - E_x\nabla E_x^*)\mathbf{e}\right. \\ & \left. + \frac{\mathrm{Re}\sigma}{4\omega}(E_x^*\nabla_\perp E_x + E_x\nabla_\perp E_x^*)\mathbf{e}\right]\mathbf{z}, \end{aligned} \tag{15}$$

where $\mathbf{e} = \mathrm{y}\mathbf{x} - \mathrm{x}\mathbf{y}$. Expression (15), which follows from the general expression (6), absent in Ref. [2], is also absent in this classical paper. Further, Eq. (15) allows obtaining the angular momentum density of a circularly polarized paraxial optical vortex with the amplitude described by Eq. (7). To do this, it is convenient to use the polar coordinate system and use Eq. (8) along with the following transition formulas:

$$\begin{aligned} \mathbf{x} &= \cos\varphi\mathbf{r} - \sin\varphi\boldsymbol{\varphi}, \\ \mathbf{y} &= \sin\varphi\mathbf{r} + \cos\varphi\boldsymbol{\varphi}, \\ \frac{\partial}{\partial x} &= \cos\varphi\frac{\partial}{\partial r} - \sin\varphi\frac{\partial}{r\partial\varphi}, \\ \frac{\partial}{\partial y} &= \sin\varphi\frac{\partial}{\partial r} + \cos\varphi\frac{\partial}{r\partial\varphi}, \\ \mathbf{e} &= -r\boldsymbol{\varphi},\ \ \mathbf{e}\nabla = -\frac{\partial}{\partial\varphi},\ \ \mathbf{e}\nabla_\perp = -r\frac{\partial}{\partial r}. \end{aligned} \tag{16}$$

Then, instead of Eq. (15), we obtain the angular momentum density for an optical vortex:

$$\begin{aligned}\mathbf{j} = {} & \frac{-z}{2\omega}\left[\frac{n}{r}(1+|\sigma|^2)|A(r,z)|^2 - \mathrm{Re}\sigma\frac{\partial|A(r,z)|^2}{\partial r}\right]\mathbf{r} \\ & + \frac{1+|\sigma|^2}{2c}\left[\frac{z}{2}F - |A(r,z)|^2 r\right]\boldsymbol{\varphi} \\ & + \frac{1}{2\omega}\left[n(1+|\sigma|^2)|A(r,z)|^2 - \mathrm{Re}\sigma r\frac{\partial}{\partial r}|A(r,z)|^2\right]\mathbf{z}. \end{aligned} \tag{17}$$

In Eq. (17), the function F is the same as in Eq. (9). It is seen in Eq. (17) that in the case of circular polarization ($\sigma = \pm 1$), the axial projection of the AM density can change its sign depending on the radial coordinate r:

$$j_z = \frac{1}{\omega}\left[n|A(r,z)|^2 - \frac{\sigma r}{2}\frac{\partial|A(r,z)|^2}{\partial r}\right]. \tag{18}$$

If the topological charge is positive ($n > 0$), then in the case of right-handed polarization ($\sigma > 0$), the AM projection (18) can be negative ($j_z < 0$) at those points in the cross section of the optical vortex, where the radial derivative of the intensity $I = |A(r,z)|^2$ is positive ($\partial I/\partial r > 0$). Vice versa, for left-handed polarization ($\sigma < 0$) the AM projection (18) can be negative ($j_z < 0$) in those areas of the transverse section of the optical vortex, where the radial derivative of the intensity is negative ($\partial I/\partial r < 0$). For a linearly polarized optical vortex ($\sigma = 0$), the AM density (17) is positive ($j_z > 0$) everywhere in the beam cross section if the topological charge is positive ($n > 0$).

Thus, it is shown that the longitudinal projection of the AM density of a circularly polarized paraxial optical vortex can change its sign and be equal to zero for any topological charge n. For optical micromanipulation, this means that a microscopic particle, trapped at different distances from the beam center, rotates either clockwise or counterclockwise. A similar property was previously observed in the vectorial Hankel beams with circular polarization [15] and in sharply focused Gaussian vortices [7]. We note that this phenomenon is similar for paraxial and nonparaxial light fields.

For circular polarization, the radii, where the axial projection of the angular momentum (18) changes its sign and where $j_z = 0$, can be found from the following equation:

$$2n|A(r,z)|^2 = \sigma r\frac{\partial|A(r,z)|^2}{\partial r}. \tag{19}$$

Note that Eq. (19) coincides with Eq. (13): Where the direction of rotation of beam energy changes, axial AM projection there changes direction as well. For example, for the Bessel beam $A(r) = J_n(k_r r)$, where $J_n(x)$ is the nth-order Bessel function of the first kind and k_r is the transverse component of the wave vector, Eq. (19) reads as

$$\frac{n}{\sigma}J_n(k_r r) = r\frac{\partial J_n(k_r r)}{\partial r}. \tag{20}$$

From Eq. (20) it follows that the axial projection of the AM is negative, $j_z < 0$ (if $n/\sigma > 0$), when

$$J_n(k_r r)[(1-\sigma)J_{n-1}(k_r r) + (1+\sigma)J_{n+1}(k_r r)] < 0;$$

i.e., $J_n(k_r r)J_{n+1}(k_r r) < 0$ for right circular polarization and $J_n(k_r r)J_{n-1}(k_r r) < 0$ for left circular polarization. It is known that the zeros of the Bessel functions of the adjacent orders are interlacing (expression 9.5.2 in Ref. [17]):

$$\gamma_{\nu,1} < \gamma_{\nu+1,1} < \gamma_{\nu,2} < \gamma_{\nu+1,2} < \gamma_{\nu,3} < \cdots,$$

where $\gamma_{\nu,m}$ is the mth zero of the νth-order Bessel function. Therefore, for right circular polarization the angular tractor can be observed for the radii $\gamma_{n,m} < k_r r < \gamma_{n+1,m}$ ($m = 1,2,\ldots$), i.e., on the inner sides of the light rings (starting from the second ring), while for left circular polarization it happens at

$\gamma_{n-1,m} < k_r r < \gamma_{n,m}$ ($m = 1,2,\ldots$), i.e., on the outer sides of the light rings (starting from the first one).

Note that the radial and longitudinal components of the AM density vector in Eq. (17) differ only by the factor $-(z/r)$. It follows from this property that on the radii, determined by Eq. (19), simultaneously with the longitudinal component of the AM its radial component also changes its sign. That is, the azimuthal projection of the linear momentum in Eq. (9), which shows rotation of the light energy flux around the optical axis, produces not only the axial projection of the AM (17), but produces radial projection in the cylindrical coordinate system as well. Similarly to the axial projection of the AM and the azimuthal projection of the linear momentum, radial projection of the AM changes sign at the same radii determined by Eqs. (13) or (19).

From Eq. (19), another interesting property of the AM density follows, which has not been noted before: Maximal value of the axial projection of the AM density j_z does not coincide with the maximal value of the intensity in the beam cross section. Indeed, from Eq. (18), an equation follows for finding the extrema j_z:

$$\left(\frac{2n}{\sigma} - 1\right)\frac{\partial I}{\partial r} = r\frac{\partial^2 I}{\partial r^2}. \tag{21}$$

It follows from Eq. (21) that the axial AM density has a maximal positive value at a radius greater than the radius of the first maximum of intensity ($\partial I/\partial r = 0$), on which $\partial^2 I/\partial r^2 < 0$ (for $n/\sigma > 0$).

Using Eq. (17), we obtain the total AM of an elliptically polarized paraxial optical vortex (let $F = 0$):

$$\mathbf{L} = \int_0^\infty \int_0^{2\pi} \mathbf{j} r dr d\varphi. \tag{22}$$

In cylindrical coordinates, we get

$$\begin{aligned} L_r &= -\pi\frac{z}{\omega}[n(1+|\sigma|^2) + \mathrm{Re}\sigma]\int_0^\infty I(r,z)dr, \\ L_\varphi &= -\pi\frac{1+|\sigma|^2}{c}\int_0^\infty I(r,z)r^2 dr, \\ L_z &= \pi\frac{n(1+|\sigma|^2) + 2\mathrm{Re}\sigma}{\omega}\int_0^\infty I(r,z)r dr. \end{aligned} \tag{23}$$

It follows from Eq. (23) that for the modal laser beams (Bessel beams [3]) with the infinite time-averaged energy (or power),

$$W = \frac{1+|\sigma|^2}{2}2\pi\int_0^\infty I(r)r dr \to \infty, \tag{24}$$

all three AM components (23) are also infinite. However, if we consider the AM, normalized by the energy (24), then only the azimuthal component remains infinite,

$$\frac{L_\varphi}{W} = -\frac{1}{c}\frac{\int_0^\infty I(r,z)r^2 dr}{\int_0^\infty I(r,z)r dr} \to \infty, \tag{25}$$

while the radial AM component is zero,

$$\frac{L_r}{W} = -\frac{z}{\omega}\left(n + \frac{\mathrm{Re}\sigma}{1+|\sigma|^2}\right)\frac{\int_0^\infty I(r,z)dr}{\int_0^\infty I(r,z)r dr} \to 0, \tag{26}$$

and only the longitudinal AM component has finite value,

$$\frac{L_z}{W} = \frac{1}{\omega}\left(n + \frac{2\mathrm{Re}\sigma}{1+|\sigma|^2}\right), \tag{27}$$

and for circular polarization it is proportional to $(n \pm 1)$.

It also follows from Eq. (27) that the longitudinal AM component of a paraxial optical vortex is propagation invariant, since it is independent of z. In particular, for linear ($\sigma = 0$) and circular ($\sigma = \pm 1$) polarization we get a simple expression, coinciding with that obtained in Ref. [2]:

$$\frac{L_z}{W} = \frac{n+\sigma}{\omega}.$$

It follows from Eq. (27) that for elliptical polarization ($\sigma = \gamma e^{i\beta}$, $\gamma \geqslant 0$, $0 < \beta < 2\pi$) the AM is fractional and can have any values in the range from $(n-1)/\omega$ to $(n+1)/\omega$.

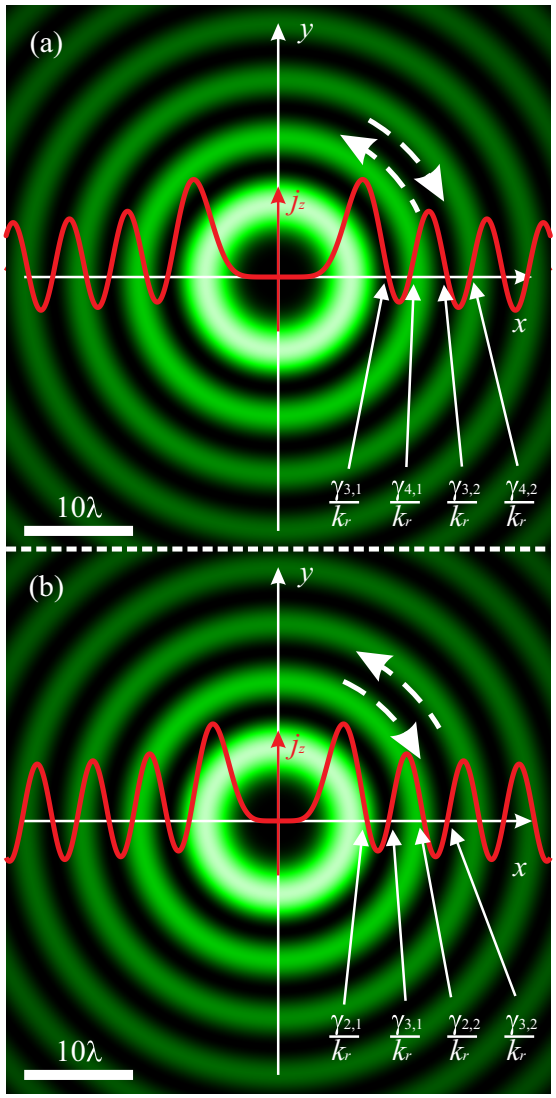

FIG. 1. Intensity distributions of the third-order Bessel modes ($n = 3$) with the scaling factor $k_r = k/10$ (i.e., paraxial beam) with right ($\sigma = 1$) (a) and left ($\sigma = -1$) (b) circular polarization. Size of the calculation area is $2R = 50\lambda$. Plots (red solid curves) show the longitudinal component of the angular momentum density vector. Dashed arrows show the direction of rotation of the energy flux.

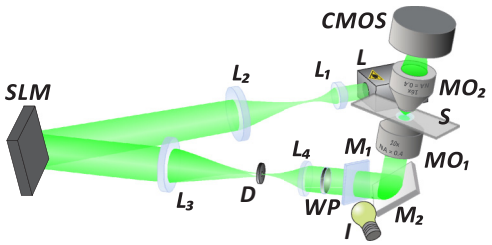

FIG. 2. Experimental setup: L is a solid-state laser ($\lambda = 532$ nm), L_1, L_2, L_3, L_4 are lenses with focal lengths ($f_1 = 150$ mm, $f_2 = 350$ mm, $f_3 = 350$ mm, $f_4 = 150$ mm), SLM is a spatial light modulator (HOLOEYE, PLUTO-VIS), D is a diaphragm, WP is a quarter-wave plate, M_1 and M_2 are mirrors, MO_1 is a micro-objective (20×, NA = 0.4), MO_2 (16×, NA = 0.3), S is a substrate with a solution of 5-μm polystyrene spheres, I is a LED bulb, CMOS is a video camera.

For nonmodal finite-energy vortex beams, for example, for the circularly polarized Gaussian vortex with the initial amplitude,

$$E_x(r,\varphi) = \exp\left(-\frac{r^2}{\delta^2} + in\varphi\right), \quad E_y = i\sigma E_x, \qquad (28)$$

where δ is the Gaussian beam waist radius, instead of Eq. (26) we get that in the initial plane all three projections of the total AM are finite:

$$L_r = 0, \quad L_\varphi = -\frac{1}{2c}\left(\frac{\pi\delta}{2}\right)^{3/2}, \quad L_z = \frac{\pi\delta^2}{2}\frac{n+\sigma}{\omega}. \qquad (29)$$

IV. NUMERICAL SIMULATION

Figure 1 shows the intensity distribution of the Bessel mode for the following parameters: wavelength $\lambda = 532$ nm; topological charge $n = 3$; scaling factor (transverse component of the wave vector) of the Bessel beam $k_r = k/10$; polarization—right-handed ($\sigma = 1$) [Fig. 1(a)] and left-handed ($\sigma = -1$) [Fig. 1(b)]; calculation area $-R \leqslant x, y \leqslant R, R = 25\lambda$. The plots on the two-dimensional (2D) intensity distributions show the longitudinal component of the angular momentum density vector j_z. It is seen in Fig. 1 that the axial component of the angular momentum vector is negative on the inner sides of the light rings (starting with the second one) for right circular polarization and on the outer sides of the light rings (starting with the first one) for left circular polarization.

V. EXPERIMENTAL ROTATION OF POLYSTYRENE MICROSPHERES IN CIRCULARLY POLARIZED BESSEL BEAMS

Shown in Fig. 2 is the optical setup used in the experiment. A linearly polarized laser beam with Gaussian intensity distribution was expanded by lenses L_1 and L_2 ($f_1 = 150$ mm, $f_2 = 350$ mm) and then directed to the spatial light modulator *SLM* (HOLOEYE, PLUTO-VIS). The light modulator was used to implement the phase mask $\tau(r, \varphi)$ of an element generating the third-order Bessel beam, $\tau(r,\varphi) = \mathrm{circ}(r/R)\,\mathrm{sgn}\, J_n(\alpha r)\exp(in\varphi)$, where (r, φ) are the polar coordinates, the α parameter is the scaling factor of the nth-order Bessel function $J_n(x)$, and R is the radius of the element. In addition to the obtained phase mask, a gradient phase mask was added for spatial separation of the nonmodulated zero diffraction order and the first diffraction order in which the Bessel beam was generated. Polarization of the Bessel beam was converted from linear to circular by using a quarter-wave plate *WP*. Using the lenses L_3, L_4 ($f_3 = 350$ mm, $f_4 = 150$ mm) and the mirror M_2, the phase modulated laser beam reflected from the modulator was directed to the input pupil of the micro-objective MO_1 (20×, NA = 0.4), which focused the laser beam into a solution with 5-μm polystyrene spheres on a substrate *S*. The diaphragm *D* blocked the zero diffraction order. The micro-objective MO_2 (16×, NA = 0.3) was used for imaging the trapping plane into the matrix of the complementary metal-oxide semiconductor (CMOS) camera. The trapping plane was illuminated by light from the LED bulb *I*. A semitransparent mirror M_1 was used to input the light. To attenuate the laser beam after the second micro-objective, neutral density filters were used (not shown in the figure).

Figure 3 shows the intensity distribution of the generated third-order Bessel beam with left circular polarization, and the stages of motion of particle pairs along the second and third light rings. Obviously, the particles trapped in the outer edge of the second light ring move clockwise, whereas the particles trapped in the inner edge of the third light ring move counterclockwise, i.e., opposite of the two particles in the second ring. The measured velocity of the particles was 0.9 ± 0.1 μm/s along the second ring and 0.7 ± 0.1 μm/s along the third ring. Such motion of microparticles agrees with the case shown in Fig. 1(b). The laser beam power in the trapping plane was about 80 mW.

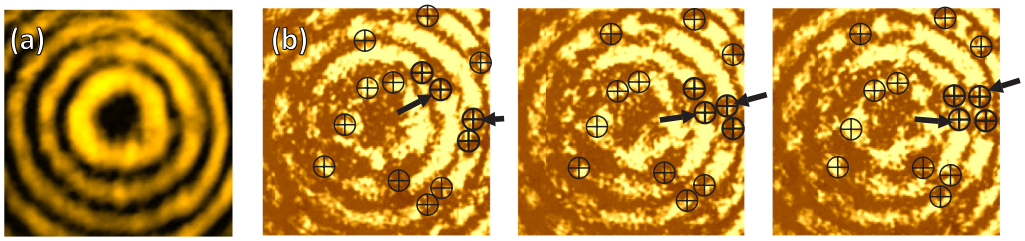

FIG. 3. Rotation of 5-μm polystyrene spheres in a third-order Bessel beam with left circular polarization: (a) intensity distribution of the laser beam in the plane of microspheres trapping, (b) stages of motion of the trapped particles (the time interval between the frames is 5 s). Frame size is 60 × 60 μm. Circles with crosses show positions of all the microspheres in each frame, while the arrows show positions of the microspheres moving in opposite directions.

VI. CONCLUSION

The following results have been obtained in this work. For an arbitrary elliptically polarized paraxial light field, an explicit expression has been obtained for the linear momentum density vector [Eq. (6)]. Earlier in Ref. [2], a partial case was obtained for the linear momentum density vector of a rotationally symmetrical light field.

As a partial case from the general expression, an expression has been obtained for the density linear momentum vector of an arbitrary optical vortex with elliptical polarization [Eq. (9)]. For linearly polarized paraxial light fields, the effect of the "optical tractor" [8] cannot take place, since for any paraxial field the axial projection of the linear momentum density vector is always greater than zero, because it is proportional to the intensity.

Using the expression for the linear momentum density of an elliptically polarized optical vortex [Eq. (9)], it has been shown that for circularly polarized paraxial optical vortices there is an effect of the "angular tractor" [Eq. (13)], when at some radius from the optical axis, the azimuthal projection of the linear momentum density vector changes its sign. This effect of the "angular tractor" means that the energy of a circularly polarized optical vortex propagates either along the right or along the left spiral at different distances from the optical axis. Also, an explicit expression for the angular momentum density vector [Eq. (15)] has been obtained for an arbitrary paraxial light field with elliptical polarization. From this expression, a simpler expression follows for the angular momentum of an arbitrary elliptically polarized optical vortex [Eq. (17)]. Equation (17) also confirms that for circular polarization the "angular tractor" effect takes place; that is, the axial projection of the angular momentum density vector changes its sign at certain distances from the optical axis. Moreover, the equation for the radii, on which the azimuthal projection of the linear momentum changes its sign [Eq. (13)], coincides with the equation [Eq. (19)], which determines the change of the sign of the axial projection of the angular momentum. In addition, an interesting property of a circularly polarized paraxial optical vortex follows from the obtained expressions: Local intensity maxima and local maxima of the axial projection of the angular momentum do not coincide and lie on different radii [Eq. (21)]. Using a spatial light modulator, a third-order Bessel beam with left circular polarization was experimentally generated and it was shown that particles trapped in the outer edge of the second light ring move clockwise, whereas the particles trapped in the inner edge of the third light ring move counterclockwise.

ACKNOWLEDGMENTS

This work was supported by the Russian Science Foundation (Project No. 17-19-01186) in the parts "Angular momentum of a paraxial laser beam" and "Numerical simulation" and by the Federal Agency for Scientific Organizations (Agreement No. 007-Г3/43363/26) in the part "Linear momentum of a paraxial laser beam." Experimental investigation performed by A.P.P. was funded by the Russian Federation Presidential grant for support of young candidates of sciences (Grant No. MK-2390.2017.2).

[1] M. J. Padgett, Orbital angular momentum 25 years on, Opt. Express **25**, 11265 (2017).

[2] L. Allen, M. Beijersbergen, R. Spreeuw, and J. Woerdman, Orbital angular momentum of light and the transformation of Laguerre-Gaussian laser modes, Phys. Rev. A **45**, 8185 (1992).

[3] L. Allen and M. Babiker, Spin-orbit coupling in free-space Laguerre-Gaussian light beams, Phys. Rev. A **53**, R2937 (1996).

[4] S. M. Barnett and L. Allen, Orbital angular momentum and nonparaxial light-beam, Opt. Commun. **110**, 670 (1994).

[5] K. Volke-Sepulveda, V. Garces-Chavez, S. Chavez-Cedra, J. Arlt, and K. Dholakia, Orbital angular momentum of a high-order Bessel light beam, J. Opt. B: Quantum Semiclassical. Opt. **4**, S82(2002).

[6] T. A. Nieminen, A. B. Stilgoe, N. R. Heckenberg, and H. Rubinsztein-Dunlop, Angular momentum of a strongly focused Gaussian beam, J. Opt. A: Pure Appl. Opt. **10**, 115005 (2008).

[7] P. B. Monteiro, P. A. Maia Neto, and H. M. Nessenzveig, Angular momentum of focused beams: Beyond the paraxial approximation, Phys. Rev. A **79**, 033830 (2009).

[8] A. V. Novitsky and D. V. Novitsky, Negative propagation of vector Bessel beams, J. Opt. Soc. Am. A **24**, 2844 (2007).

[9] S. S. R. Oemrawsingh, E. R. Eliel, G. Nienhuis, and J. P. Woerdman, Intrinsic orbital angular momentum of paraxial beams with off-axis imprinted vortices, J. Opt. Soc. Am. A **21**, 2089 (2004).

[10] A. Cerjan and C. Cerjan, Orbital angular momentum of Laguerre-Gaussian beams beyond the paraxial approximation, J. Opt. Soc. Am. A **28**, 2253 (2011).

[11] V. V. Kotlyar and A. A. Kovalev, Circularly polarized Hankel vortices, Opt. Express **25**, 7778 (2017).

[12] G. Q. Zhou, X. G. Wang, C. Q. Dai, and X. X. Chu, Angular momentum density of a Gaussian vortex beam, Sci. China-Phys. Mech. Astron. **57**, 619 (2014).

[13] K. Cheng, G. Lu, and X. Zhong, The Poynting vector and angular momentum density of Swallowtail-Gauss beams, Opt. Commun. **396**, 58 (2017).

[14] Y. Zhu, X. Liu, J. Gao, Y. Zhang, and F. Zhao, Probability density of the orbital angular momentum mode of Hankel-Bessel beams in an atmospheric turbulence, Opt. Express **22**, 7765 (2014).

[15] V. V. Kotlyar, A. A. Kovalev, and V. A. Soifer, Hankel-Bessel laser beams, J. Opt. Soc. Am. A **29**, 741 (2012).

[16] K. Y. Bliokh and F. Nori, Transverse and longitudinal angular momenta of light, Phys. Rep. **592**, 1 (2015).

[17] M. Abramowitz and I. A. Stegun, *Handbook of Mathematical Functions*, Applied Mathematics Series Vol. 55 (National Bureau of Standards, Washington, DC, 1979).